Unsteady Aligned MHD Boundary Layer Flow and Heat Transfer of a Magnetic Nanofluids Past an Inclined Plate

Mohd Rijal Ilias[1,2], Nur Sa'aidah Ismail[1], Nurul Hidayah Ab Raji[1], Noraihan Afiqah Rawi[2], Sharidan Shafie[2]
[1] Faculty of Computer and Mathematical Sciences, Universiti Teknologi MARA, Malaysia
[2] Department of Mathematical Sciences, Faculty of Science, Universiti Teknologi Malaysia, Johor Bahru, Malaysia
Email: rijal_rs@hotmail.com, nursaaidah@salam.uitm.edu.my, hidayah417@perlis.uitm.edu.my, nafiqah38@gmail.com, sharidan@utm.my

***Abstract*— A theoretical study has been done on the unsteady aligned MHD boundary layer flow as well as magnetic nanofluid's heat transfer through an inclined plate with leading edge accretion. For conventional base fluid, water and kerosene were used as they contain magnetite (Fe_3O_4) nanoparticles. Magnetic (Fe_3O_4) and non-magnetic (Al_2O_3) nanoparticles are compared as well. The governing partial differential equations are reduced into nonlinear ordinary differential equations through a suitable similarity transformation, where the Keller box method is used to solve numerically. Graphical and tabular results are discussed quantitatively in terms of the impact of pertinent parameters like magnetic parameter, M, magnetic field inclination angle, α, angle of plate inclination, γ nanoparticles volume fraction, ϕ and free convection parameter, Gr_x ,on the dimensionless velocity, skin friction coefficient, temperature and heat transfer rate. The outcomes indicate that the leading-edge accretion can significantly alter the fluid motion and the heat transfer attributes.**

***Index Terms*— unsteady aligned MHD, inclined plate, magnetic nanofluids, leading edge accretion**

I. Introduction

Fluid heating and cooling holds a lot of significance in several sectors, including manufacturing, power, electronics and transportation. Effectual ways of cooling are extremely essential to cool any high-energy apparatus. The usual heat transfer fluids like ethylene glycol, water and engine oil have inadequate/substandard heat transfer competences because of their limited heat transfer attributes. On the other hand, metals demonstrate thermal conductivities almost thrice more compared to those fluids. Thus, it is obvious that a blend of the two substances is highly sought to create a heat transfer medium which will perform like a fluid but exhibits a thermal conductivity of a metal. Numerous investigational and theoretic studies had been conducted to enhance the fluids' thermal conductivity. In 1993, when examining new coolants and cooling technologies at Argonne national laboratory (United States), Choi developed a new kind of fluid known as nanofluids [1]. It is a fluid which comprises tiny volumetric amounts of nanometre-sized particles known as nanoparticles. It is basically an engineered colloidal suspension of nanoparticles within a base fluid [2]. The nanoparticles utilised in nanofluids are mostly formulated from oxides, metals, carbides or carbon nanotubes. Some of the base fluids commonly used are ethylene glycol, water and oil. Nanofluids usually comprise up to 5 percent of volume fraction of nanoparticles for effectual heat transfer improvements. Nanofluids are frequently a topic of research due to their heat transfer attributes. These nanofluids help to improve the convective properties as well as thermal conductivity of the base fluid's properties. Normally, the heat transfer coefficient improved by almost 40% and thermal conductivity enhancements have been found to be in the range of 15–40% over the base fluid [3]. However, such levels of increment in thermal conductivity cannot be completely attributed to the added nanoparticles' higher thermal conductivity. Attribution behind performance enhancements could have come from other mechanisms as well. Besides, there are many other potential applications of the interaction between nanofluids and the magnetic field. One such example is that it is used to deal with issues of cooling down nuclear reactors by liquid sodium and induction flow metre that relies on the potential difference in the fluid in the direction perpendicular to the magnetic field and to the motion.

The field of magnetohydrodynamics (MHD) involving fluid mechanics includes the phenomena resulting from applying a magnetic field to an electrically conducting fluid. In recent years, the research related to the field of MHD has developed rapidly [4]. Many applications that involved an electrically conducting fluid had been derived through the study of flow and heat transfer when a magnetic field is applied past a heated surface. Some of these applications include manufacturing processes such as nuclear reactor, cooling down metallic plate and extrusion of polymers. In electrically conducting fluid, the MHD flow can also control the heat transfer rate at the surface, which results in achieving the desired cooling

Manuscript received July 1, 2018; revised August 24, 2019.

doi: 10.18178/ijmerr.9.2.197-206

effect. Although advanced nanofluids like CNT–water diamond–water is available, they are too expensive for practical uses. Thus, the more economically cheaper nanofluids were considered as alternatives, which also offered better heat transfer improvements. Ferrofluids are basically magnetic nanofluids that are normally stable liquids comprising dispersed colloidal magnetic nanoparticles like cobalt, Fe_3O_4 and nickel. Unlike conventional non-magnetic nanofluids, ferrofluids provide various advantages when employed as heat transfer media – for example, (i) the solute nanoparticles' properties (e.g. thermal conductivity and viscosity) can be modified using external magnetic field to achieve a specific design requirements, (ii) the thermomagnetic convection in a ferrofluid can be controlled and enhanced by employing the external magnetic field, and (iii) the size and cost of components can be decreased by applying ferrofluids in heat transfer devices. With respect to these superior benefits, a few researchers [5,6] had confirmed that ferrofluids gave excellent heat transfer improvements. The researchers also examined the impact of MHD on ferrofluids in a semi-circular annulus and found that the heat transfer rate improved as shown by the increase in the Rayleigh number as well as solid volume fraction. Besides that, the Hartmann number decreases showing a better heat transfer augmentation was achieved. The authors in [7] had described the various advantages of a ferrofluids on MHD convection with regards to cobalt-kerosene ferrofluids.

Sparrow et al. [8] studied the convection flow in an inclined surface, where they have explained the combined forced and free boundary layer issues by employing a similar method. In an inclined surface, the buoyancy force that triggered motion has a component in both normal and tangential directions. This resulted in generating a pressured gradient across the boundary layer, hence, making the theoretical analysis more complicated when compared with a horizontal or a vertical surface. For laminar mixed convection flow, Mucoglu and Chen [9] evaluated the buoyancy force impact on the heat transfer characteristics in an inclined flat surface that was either exposed to a uniform heat flux or maintained at a constant temperature. In the main flow analysis, Cheng [10] examined the mixed convection boundary layer flow in an inclined plate by administering the normal component of buoyancy force that generates stream-wise pressure gradient in the flow. Inclined at an angle of $45°$ towards the vertical, he obtained numerical solutions for isothermal plate, ignoring the buoyancy force component normal to the inclined plate. Many investigators [11-15] have studied hydromagnetic boundary layer flow in an inclined plate by considering different physical conditions. Chen [16] evaluated MHD natural convection flow's heat, momentum and mass transfer characteristics over a permeable, inclined surface with varying concentration and wall temperature, by taking into account the impact of viscous dissipation and ohmic heating. The influence of variable viscosity and magnetic field was examined by Seddeek [17] for the flow and heat transfer over a continuously moving porous plate. The issue of unsteady natural convection flow was investigated by Ganesan and Palani [18] for a viscous incompressible electrically conducting fluid over an inclined plate that has variable heat and mass flux, when introduced to a magnetic field.

Todd [19] presented a new unsteady boundary layer problem that included the moving leading edge with a specific rate of accretion or ablation and Fang [30] did some additional analysis for the thermal boundary layers and momentum. This paper's goal acts as an extension to the study of Todd [19] and Fang [20] for a magnetic nanofluid's unsteady aligned MHD boundary layer past along an inclined plate. Moreover, comparison is made between non-magnetic (Al_2O_3) and magnetic (Fe_3O_4) nanoparticles.

II. Mathematical Formulation

Unsteady, two-dimensional laminar boundary layer flow of a nanofluid past an inclined plate with an acute angle γ to the vertical is considered. The unsteadiness is caused by the steady rate of accretion at the leading edge. Let U_∞ signify the uniform free stream velocity and T_∞ represent free stream temperature. The $x-$axis is taken vertically up towards the direction of free stream, while $y-$axis would be perpendicular to the free stream. To the flow, with acute angle, α, the aligned magnetic field is applied and it is expected to be a function of the distance from the origin denoted as $B(x) = B_o / \left((\cos\omega)\nu_f \tau + (\sin\omega)\left(\frac{\nu_f x}{U_\infty}\right)\right)^{1/2}$ with $B_o \neq 0$, where the coordinate along the plate is x. In all these studies, nanofluid is assumed to be incompressible, and the viscous dissipation, radiation and chemical reaction effects are neglected. Nanofluids are assumed to behave as single-phase fluids with local thermal equilibrium between the base fluid and the nanoparticles suspended in them so that no slip occurs between them. The fluid used are water and kerosene-based nanofluid, which contain two different types of nanoparticles, i.e. alumina and magnetite. Table I presents the thermophysical properties. Fig. 1 provides a schematic diagram of the problem.

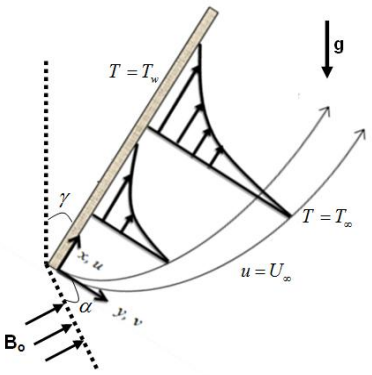

Figure 1. Flow configuration.

The nanofluids equation model as presented by Tiwari and Das [21] is been used for this study. This model is developed to analyze the behaviour of nanofluids taking

into account the solid volume fraction. The governing equations for motion and heat transfer characteristics for unsteady flow are:

$$\frac{\partial u}{\partial x}+\frac{\partial v}{\partial y}=0 \tag{1}$$

$$\frac{\partial u}{\partial t}+u\frac{\partial u}{\partial x}+v\frac{\partial u}{\partial y}=\frac{\mu_{nf}}{\rho_{nf}}\frac{\partial^2 u}{\partial y^2} + \frac{(\rho\beta)_{nf}}{\rho_{nf}}g(T-T_\infty)\cos\gamma-\frac{\sigma B^2(x)}{\rho_{nf}}\sin^2\alpha(u-U_\infty) \tag{2}$$

$$\frac{\partial T}{\partial t}+u\frac{\partial T}{\partial x}+v\frac{\partial T}{\partial y}=\alpha_{nf}\frac{\partial^2 T}{\partial y^2} \tag{3}$$

Boundary conditions of these equations are

$$\begin{aligned} &u=0,\ v=0,\ T=T_w && \text{at} && y=0,\\ &u\to U_\infty,\quad T\to T_\infty && \text{as} && y\to\infty. \end{aligned} \tag{4}$$

where u and v are velocity components in x and y directions, T is local temperature of nanofluid, g is acceleration due to gravity and σ is the electrical conductivity. Thermophysical properties of nanofluids, namely, ρ_{nf} is the effective density, μ_{nf} is the effective dynamic viscosity, $(\rho\beta)_{nf}$ is the thermal expansion coefficient and α_{nf} is the thermal diffusivity are given by

$$\begin{aligned} &\rho_{nf}=(1-\phi)\rho_f+\phi\rho_s,\ \mu_{nf}=\frac{\mu_f}{(1-\phi)^{2.5}},\\ &(\rho\beta)_{nf}=(1-\phi)(\rho\beta)_f+\phi(\rho\beta)_s,\ \alpha_{nf}=\frac{k_{nf}}{(\rho C_p)_{nf}}. \end{aligned} \tag{5}$$

Here, ϕ is the solid volume fraction, μ_f is the dynamic viscosity of the base fluid, ρ_f and ρ_s are the densities of pure fluid and nanoparticles, respectively. $(\rho C_p)_{nf}$ is the heat capacity of the nanofluid and k_{nf} is the thermal conductivity of the nanofluid given by

$$\begin{aligned} &(\rho C_p)_{nf}=(1-\phi)(\rho C_p)_f+\phi(\rho C_p)_s,\\ &\frac{k_{nf}}{k_f}=\frac{k_s+2k_f-2\phi(k_f-k_s)}{k_s+2k_f+\phi(k_f-k_s)}. \end{aligned} \tag{6}$$

where $(\rho C_p)_f$ and $(\rho C_p)_s$ are the specific heat parameters of the base fluid and nanoparticles. k_f and k_s are thermal conductivities of the nanofluid and nanoparticles. The viscosity of the ferrofluid μ_{nf} can be approximated as the viscosity of a base fluid μ_f containing dilute suspension of fine spherical particles and is given by Brikmann [22]. The effective thermal conductivity of the nanofluid k_{nf} is approximated by Maxwell-Garnett's model, which is found to be appropriate for studying heat transfer enhancement using nanofluid. Consider the following stream function as used in [19,20,23,24]

$$\psi(x,y,t)=U_\infty\left((\cos\omega)\nu_f\tau+(\sin\omega)\left(\tfrac{\nu_f x}{U_\infty}\right)\right)^{1/2}f(\eta) \tag{7}$$

with the similarity variable (referred to as the Blasius–Rayleigh–Stokes variable in [29])

$$\eta=\frac{y}{\left((\cos\omega)\nu_f\tau+(\sin\omega)\left(\tfrac{\nu_f x}{U_\infty}\right)\right)^{1/2}} \tag{8}$$

and a nondimensional temperature $\theta=\theta(\eta)$ as

$$\theta(\eta)=\frac{T-T_\infty}{T_w-T_\infty} \tag{9}$$

where ω is unsteady parameter, ν_f is kinematic viscosity of fluid fraction and ψ is stream function which is defined in usual form as

$$u=\frac{\partial\psi}{\partial y}\ \text{ and }\ v=-\frac{\partial\psi}{\partial x} \tag{10}$$

In terms of these new variables, the velocity components can be expressed as

$$\begin{aligned} &u=U_\infty f'(\eta)\\ &v=\left(\frac{\nu_f}{2}\right)\frac{(\eta f'-f)\sin\omega}{\left((\cos\omega)\nu_f\tau+(\sin\omega)\left(\tfrac{\nu_f x}{U_\infty}\right)\right)^{1/2}} \end{aligned} \tag{11}$$

Using (7) - (11) into (1) - (4), the momentum and energy equations together with the boundary conditions can be written as

$$\begin{aligned} f'''+\frac{1}{2}(1-\phi)^{2.5}\left(1-\phi+\left(\frac{\phi\rho_s}{\rho_f}\right)\right)(\eta\cos\omega+f\sin\omega)f'' \\ +(1-\phi)^{2.5}M\sin^2\alpha(1-f') \\ +(1-\phi)^{2.5}\left(1-\phi+\phi\frac{(\rho\beta)_s}{(\rho\beta)_f}\right)Gr_x\theta\cos\gamma=0 \end{aligned} \tag{12}$$

$$\frac{k_{nf}}{k_f}\theta''+\frac{\Pr}{2}(\eta\cos\omega+f\sin\omega)\theta'=0 \tag{13}$$

with the boundary conditions

$$\begin{aligned} &f(0)=0,\quad f'(0)=0,\quad \theta(0)=1,\\ &f'(\eta)\to1,\quad \theta(\eta)\to0,\ \text{as}\ \ \eta\to\infty \end{aligned} \tag{14}$$

Here the primes denote differentiations with respect to similarity variable η. The corresponding dimensionless group that appears in the governing equations are defined by: $\Pr=\nu_f/\alpha_f$ is the Prandtl number, $Gr_x=\left((\cos\omega)\nu_f\tau+(\sin\omega)\left(\tfrac{\nu_f x}{U_\infty}\right)\right)g\beta_f(T_w-T_\infty)/\nu_f U_\infty^{\,2}$ is the free convection parameter [24], $M=\sigma B_o^{\,2}/\rho_f$ is the magnetic interaction parameter.

The quantities of physical interest in this work are the local Skin friction coefficient C_f and the local Nusselt number Nu_x are defined as

$$C_f=\frac{\tau_w}{\rho_f U_\infty^{\,2}}\quad\text{and}\quad Nu=\frac{xq_w}{k_f(T_w-T_\infty)} \tag{15}$$

where τ_w is the skin friction or the shear stress and q_w is the heat flux from the plate. τ_w and q_w are given by

$$\tau_w = \mu_{nf}\left(\frac{\partial u}{\partial y}\right)_{y=0} \quad \text{and} \quad q_w = -k_{nf}\left(\frac{\partial T}{\partial y}\right)_{y=0} \tag{16}$$

Substituting (7) - (9) into (15) and (16), the skin friction and reduced Nusselt number can be written as

$$\mathrm{Re}_x^{1/2} C_f = \frac{1}{(1-\phi)^{2.5}} \frac{f''(0)}{(\cos\omega)\tau + \sin\omega}$$

and (17)

$$\mathrm{Re}_x^{-1/2} Nu = -\frac{k_{nf}}{k_f} \frac{\theta'(0)}{\left((\cos\omega)\tau + \sin\omega\right)^{1/2}}$$

where $\mathrm{Re}_x = U_\infty x/\nu_f$ is the local Reynolds number and the non-dimensional time variable $\tau = U_\infty t/x$ [25].

III. Numerical Solution

Equations (12) and (13) subject to the boundary conditions (14) are solved numerically using Keller-box [26] method as described in the books by Cebeci and Bradshaw [27]. The solution can be obtained in the following four steps.

1. Reduce (12) and (13) to first-order system.
2. Write the difference equations using central differences.
3. Linearize the resulting algebraic equations by Newton's method and write them in the matrix-vector form.
4. Solve the linear system by the block tridiagonal elimination technique.

IV. Results and Discussion

If the free convection parameter is not present, $Gr_x = 0$, magnetic parameter, $M = 0$, with no further addition of nanoparticles, $\phi = 0$, the system of equations contains solutions that lie in the range of $-\frac{\pi}{4} \le \omega < \frac{3\pi}{4}$, which is comparable to the results achieved in [19,20]. When $0 < \omega \le \frac{\pi}{2}$, a leading edge accretion can be maintained with a rate of $U_\infty \cot\omega$, specifically the leading edge progressing upstream. When $\frac{\pi}{2} < \omega \le \omega_o$, where $\omega_o \approx 104.655°$ [20], a leading edge ablation occurs with a rate of $|U_\infty \cot\omega|$. When $-\frac{\pi}{4} \le \omega < 0$, a "backward" boundary layer may be present with trailing edge accretion. At the critical points $\omega = 0$ and $\omega = \frac{\pi}{2}$, the results can be seen similar to that of the well-known Rayleigh–Stokes problem and Blasius flat plate boundary layers, respectively. Blasius-Rayleigh-Stokes boundary layers are considered for all other solutions that lie in the range of $0 < \omega < \frac{\pi}{2}$. Since the analytical solutions presented in (12) and (13) are unavailable, the problem has to be solved by employing different numerical techniques. For different parameters, the similarity equations have to be solved. The code was validated against the previous results prior to obtaining the final results.

To examine the behaviour of velocity and temperature profiles in terms of the physical problem, various values will carry numerical calculations, including magnetic field inclination angle, α, magnetic interaction, M, angle of plate inclination, γ, free convection parameter, Gr_x and nanoparticles volume fraction, ϕ. For numerical computations, some of the non-dimensional values remain fixed, such as $\alpha = 90°, \gamma = 45°, M = 2, \phi = 0.05$ and $Gr_x = 1$. In the entire analysis, these values are treated to be common, excluding the different displayed values in specific tables and figures.

TABLE I. Thermophysical Properties of Base Fluids and Ferroparticle [28, 29, 30].

Physical Properties	Water	Kerosene	Fe_3O_4	Al_2O_3
$\rho(kg/m^3)$	997.1	780	5200	3970
$C_p(J/kgK)$	4179	2090	670	765
$k(W/mK)$	0.613	0.149	6	40
$\beta\times10^{-5}(K^{-1})$	21	99	1.3	0.85
Pr	6.2	21		

TABLE II. Comparison of $-\theta(0)$ Values for Different Values of Pr When $\omega = \pi/2, Gr_x = 0, M = 0, \phi = 0$ (Pure Fluid).

Pr	Bejan [31]	Present study
0.7	0.292	0.292683
0.8	0.307	0.306918
1	0.332	0.332059
5	0.585	0.576696
6.2 (water)	---	0.620077
10	0.730	0.728155
21(kerosene)	---	0.933538

For different Pr values, Table II shows the comparison of $-\theta'(0)$ with Bejan [31]. Moreover, Table III gives a of the values given by Todd [19] for different values of ω. Based on Table III, it is seen that there is an increase in the skin friction coefficient with increasing ω. It is also observed that magnetic nanofluids have much more higher skin friction when compared to on-magnetic nanofluid and pure fluid. The comparisons are found to be in an excellent agreement as shown.

TABLE III. COMPARISON OF $f''(0)$ VALUES FOR DIFFERENT VALUES OF ω WHEN $\omega=\pi/2, Gr_x=0, \gamma=90°, M=0$.

Accretion rate (approximation)	ω	Pure fluid		Magnetic Nanofluid ($\phi=0.05$)		Non-Magnetic Nanofluid ($\phi=0.05$)	
		Todd [19]	Present Study	Fe_3O_4-water	Fe_3O_4-kerosene	Al_2O_3-water	Al_2O_3-kerosene
Rayleigh-Stokes	0	0.5642	0.564191	0.661912	0.681462	0.644832	0.660196
$(7.596)U_\infty$	$\pi/24$	0.5750	0.575018	0.673678	0.692736	0.657047	0.672006
$(3.732)U_\infty$	$\pi/12$	0.5807	0.580731	0.679485	0.697910	0.663424	0.677870
$(1.732)U_\infty$	$\pi/6$	0.5770	0.577004	0.673405	0.690109	0.658875	0.671943
U_∞	$\pi/4$	0.5529	0.552877	0.643446	0.657763	0.631020	0.642194
$(0.577)U_\infty$	$\pi/3$	0.5072	0.507220	0.588181	0.599310	0.578551	0.587209
$(0.268)U_\infty$	$5\pi/12$	0.4369	0.436866	0.503658	0.510452	0.497808	0.503067
$(0.132)U_\infty$	$11\pi/24$	0.3900	0.39000	0.447367	0.451264	0.444027	0.447029
Blasius	$\pi/2$	0.3321	0.332059	0.377490	0.377490	0.377490	0.377490

The velocity and temperature distribution are presented in Figs. 2 and 3 for the entire flow of the Fe_3O_4–water nanofluid as well as the effect of α. With an increase in α for $\omega=45°, 70°$ and $90°$, there is an increase in flow velocity and decrease in the boundary layer thickness. As seen in Fig. 3, there is a decrease in the temperature of the Fe_3O_4–water at a fixed point as well as the thermal boundary layer with rise in α for $\omega=45°, 70°$ and $90°$. For $\omega=0°$, there was no influence on the temperature due to variation of α. As mentioned in [19], $\omega=0°$ corresponds to Rayleigh-Stokes layer where the problem is considered as a purely diffusive boundary layer that has complete absence of convection. On the other hand, there was increased in both temperature and thermal boundary layer when $\omega=-45°$, due to an increase in α. As highlighted in [19] and [20], an unsteady boundary layer of a trailing edge accretion could occur when there is a negative value of ω. Mathematically, negative values of ω could also be presented; however, this flow did not find much practical applications and is not discussed here for other parameters.

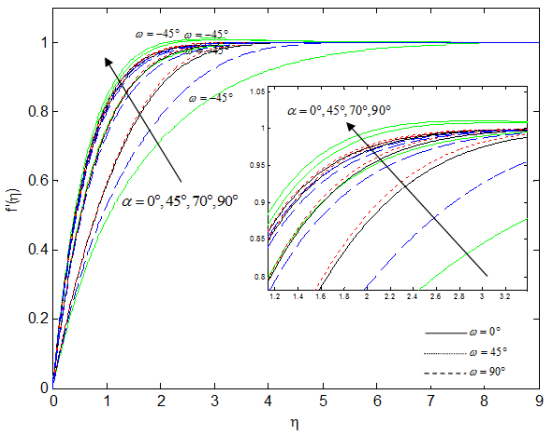

Figure 2. Effect of α on velocity for various ω.

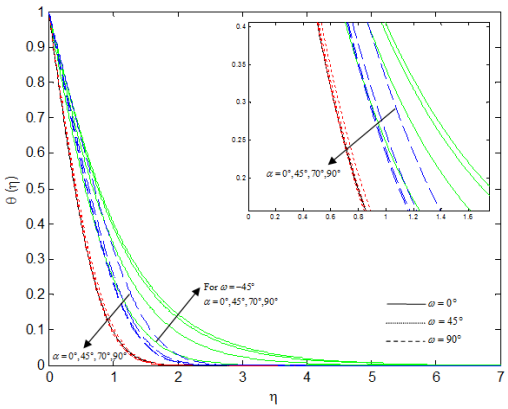

Figure 3. Effect of α on temperature for various ω.

Figs. 4 and 5 show the effect of M on the flow and temperature profiles for four different values. $M=0$ occurs for condition when the applied magnetic field is missing. As M increases in Fig. 4, velocity also accelerated in all cases of ω. It has been proven that the magnetic force allows enhancing the boundary layer as the term $(u-U_\infty)$ continues to remain positive in the momentum equation in the boundary layer region. On an increase in M, the Lorentz force associated with the boundary layer gets thinner for the magnetic field. The magnetic lines move based on the free stream velocity as they move past the plate. The magnetic field pushes the fluid that was decelerated due to viscous force, which also counteracts the viscous effects. Hence, with any increase in M for $\omega=0°, 45°$ and $90°$., the velocity of the fluid also increases. Based on Fig. 5, it is seen that the temperature decreases with increase in M in free stream conditions. A decrease in the thermal boundary layer thickness occurs with increase in M for $\omega=45°$ and $90°$. For $\omega=0°$, there was no change in the temperature.

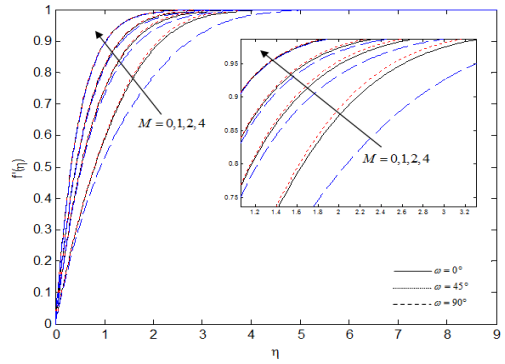

Figure 4. Effect of M on velocity for various ω.

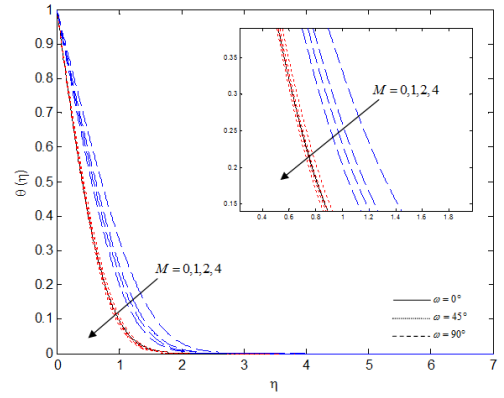

Figure 5. Effect of M on temperature for various ω.

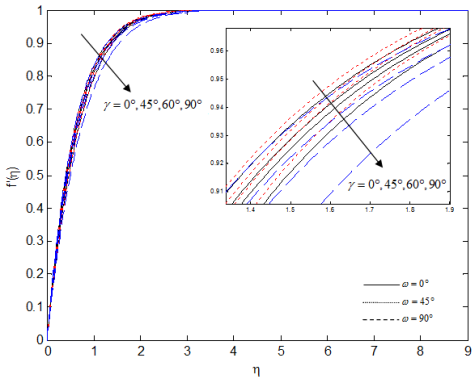

Figure 6. Effect of γ on velocity for various ω.

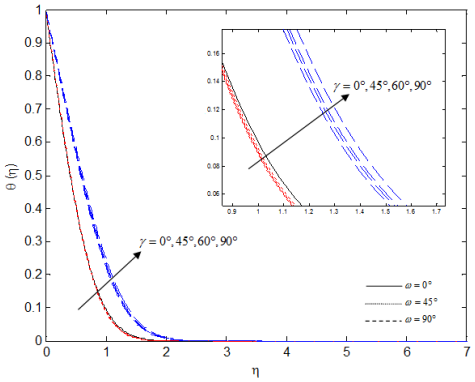

Figure 7. Effect of γ on temperature for various ω.

Figs. 6 and 7 show the variations occurring in the dimensionless velocity and temperature profiles, respectively, for diverse values of the angles of inclination $(\gamma = 0°, 45°, 60°, 90°)$. From Fig. 6, for all cases of ω, the boundary layer flow for the velocity is seen to reduce with rise in the angle of inclination. This is because the rise in the angle of inclination will cause the buoyancy force effect, which resulted from the decrease in thermal variations due to a factor of $\cos\gamma$. Also, it can be observed that the impact of the buoyancy force (which is maximum for $\gamma = 0°$) overruns the main stream velocity considerably.

As presented in Fig. 7, the temperature is seen to increase with the increase in the angle of inclination except for $\omega = 0°$. One can notice that when $\gamma = 90°$, the issue decreases to the horizontal flat plate, while the same issue decreases to the vertical flat plate when $\gamma = 0°$ and to the inclined flat plate when $\gamma = 45°$ and $60°$.

The increase in Gr_x will improve the velocity of fluid enhances for $\omega = 0°, 45°$ and $90°$ (Fig. 8). The free convection parameter, Gr_x can be positive, negative or zero. $Gr_x = 0$ indicates the absence of free convection, while $Gr_x > 0$ gives rise to the cooling problem. It implies that $T_w > T_\infty$. When $Gr_x < 0$ it implies $T_w < T_\infty$, the heat flow is from the fluid to the plate. On the other hand, the increase of Gr_x is caused by the rise in buoyancy force. This force through convection enhances the heat transfer rate. The greater convection is caused by increase in temperature, which decreases the density of the nanofluid at higher temperature. It is clear that the fluid velocity of a lesser density is greater when compared to a larger density fluid.

Fig. 9 depicts the impact of Gr_x on dimensionless temperature. It has been observed that the temperature decreases with an increase in Gr_x for $\omega = 0°, 45°$ and $90°$. It agrees to the fact that there is an increase in the fluid velocity due to buoyancy force, which then resulted a decrease in the temperature of the fluid. Also, it can be noted that there is a decrease in thermal boundary layer thickness. For $\omega = 0°$, there was no change in the temperature.

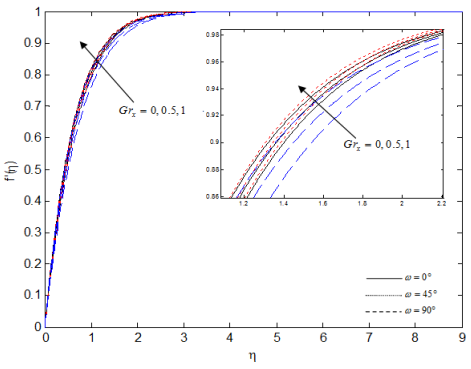

Figure 8. Effect of Gr_x on velocity for various ω.

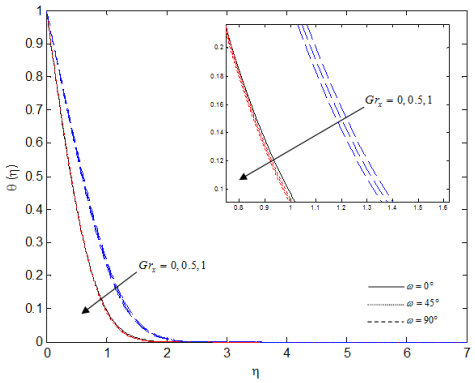

Figure 9. Effect of Gr_x on temperature for various ω.

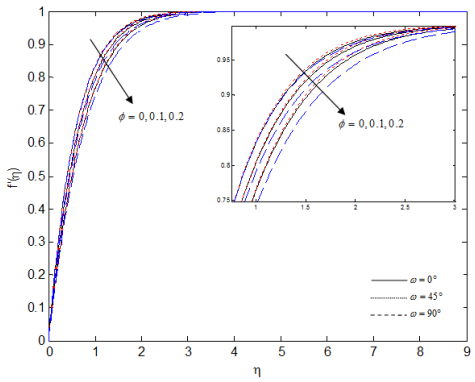

Figure 10. Effect of ϕ on velocity for various ω.

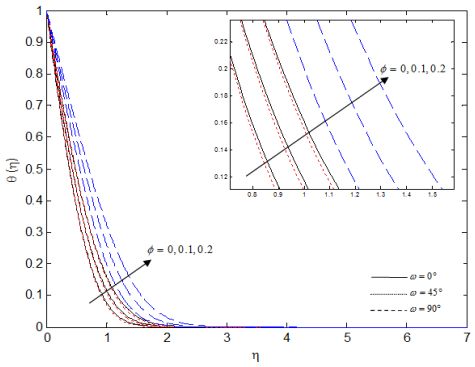

Figure 11. Effect of ϕ on temperature for various ω.

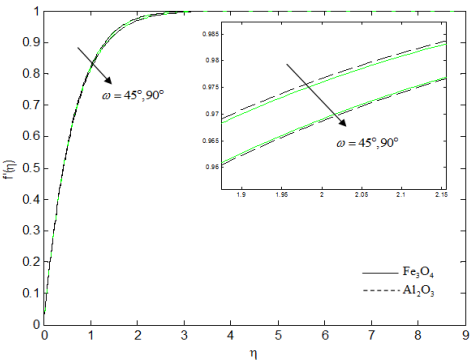

Figure 12. Comparison between magnetic nanofluid and non-magnetic nanofluid velocity when $\alpha = 90°, M = 2, Gr_x = 1, \phi = 0.05$ and $\gamma = 45°$.

Fig. 10 presents the impact caused by ϕ on the Fe_3O_4–water nanofluid's velocity. It has been confirmed that reduction in velocity occurred due to an increase in ϕ for $\omega = 0°, 45°$ and $90°$. This is because of the increase in ϕ that makes the fluid to become more viscous, causing a reduction in the velocity of the magnetic nanofluid.

Fig. 11 shows the impact of ϕ on Fe_3O_4–water nanofluid's temperature distribution. There is a continuous increment in the thermal boundary layer with the increase in nanoparticles' volume fraction that lies in the range of $0 \le \phi \le 0.20$. This is consistent with the physical behaviour where the nanofluid's thermal conductivity increases with a rise in the volume fraction of the nanoparticles, and thus the boundary layer's thickness also increases. Colla et al. [32] also reported this behaviour experimentally. This observation suggests that using Fe_3O_4–water nanofluids is advantageous in the heating and cooling processes.

Fig. 12 shows the plot for Al_2O_3–water and Fe_3O_4–water nanofluids. It was found that the Fe_3O_4–water nanofluid's temperature was lesser when compared to that of the temperature of Al_2O_3–water. The magnetic nanofluid's viscosity and thermal conductivity are both temperature dependent. Increase in temperature leads to increase in thermal conductivity, whereas viscosity is decrease when temperature increased. Moreover, the viscosity was greater for Fe_3O_4–water than for Al_2O_3–water. It was found that this graphical illustration was the same to that of the experimental results obtained by Colla [32].

Rather than the temperature profiles and shape of the velocity, focus is given more to the values of the skin friction and heat transfer for engineering and practical purposes. Thus, our interest lies in examining the important physical quantities with regards to the flow behaviour and heat transfer characteristics through the analysis of heat transfer rate and non-dimensional shear stresses at the plate. Table IV and V list the numerical values for heat transfer rate and shear stresses at the plate when $\eta = 0$ for different values of α, M, γ, Gr_x and ϕ.

Table IV depicts the numerical denominations of $f''(0)$ for various values of α, M, Gr_x and ϕ. The table also compares the magnetic and non-magnetic nanofluids. It is quite evident that the values of $f''(0)$ rise with α, M λ_T and Gr_x for $\omega = 0°, 45°$ and $90°$. Furthermor e, the ϕ propels the friction factor coefficients for each of the three cases. The nanofluids' density rises with the rise in ϕ. As a result, the skin friction rises as well. In case of $\omega = 0°$ and $45°$, the non-magnetic nanofluids friction factor coefficient is less when a comparison is done with magnetic nanofluids; however, it shows a reverse behaviour in case of $\omega = 90°$.

Table V exhibits the variation in local Nusselt for various values of non-dimensional factors. The heat transfer rates are stimulated with enhancing values of α, M, Gr_x and ϕ for $\omega = 45°$ and $90°$. In case of $\omega = 0°$,

only ϕ enhances the transfer rate whereas other parameters do not cause any impact. The Nusselt numbers increase with rising ϕ. This is due to the rise in nanofluids' thermal conductivity with respect to the escalating ϕ.The transfer rate of heat is greater in non-magnetic nanofluids than in magnetic nanofluids. As the magnetic field's strength is raised, the magnetic nanoparticles line up in one direction and demonstrate greater heat transfer rate that are analogous to non-magnetic nanoparticles.

TABLE IV. VARIATION IN SKIN FRICTION FOR MAGNETIC NANOFLUIDS AND NON-MAGNETIC NANOFLUIDS AT DIFFERENT PARAMETERS.

α	M	γ	Gr_x	ϕ	Fe_3O_4-water **Fe_3O_4-kerosene**			Al_2O_3-water **Al_2O_3-kerosene**		
					$\omega = 0°$	$\omega = 45°$	$\omega = 90°$	$\omega = 0°$	$\omega = 45°$	$\omega = 90°$
0°					0.934123	0.939614	0.877538	0.919998	0.926016	0.871454
					0.836476	**0.840874**	**0.744685**	**0.816865**	**0.822010**	**0.736226**
45°					1.465345	1.463449	1.438514	1.458310	1.456475	1.435680
	2	45°	1	0.05	**1.383608**	**1.386151**	**1.356156**	**1.374065**	**1.376951**	**1.353245**
70°					1.757533	1.753554	1.733226	1.752010	1.748068	1.730888
					1.684499	**1.685502**	**1.664555**	**1.677275**	**1.678531**	**1.662424**
90°					1.836510	1.832149	1.812552	1.831275	1.826952	1.810307
					1.765684	**1.766332**	**1.746882**	**1.758911**	**1.759797**	**1.744892**
	0				0.934123	0.939614	0.877538	0.919998	0.926016	0.871454
					0.836476	**0.840874**	**0.744685**	**0.816865**	**0.822010**	**0.736226**
	1				1.465345	1.463449	1.438514	1.458310	1.456475	1.435680
90°		45°	1	0.05	**1.383608**	**1.386151**	**1.356156**	**1.374065**	**1.376951**	**1.353245**
	2				1.836510	1.832149	1.812552	1.831275	1.826952	1.810307
					1.765684	**1.766332**	**1.746882**	**1.758911**	**1.759797**	**1.744892**
	4				2.399599	2.393853	2.377029	2.395675	2.389991	2.375208
					2.342497	**2.341297**	**2.327480**	**2.337805**	**2.336777**	**2.326107**
		0°			1.924251	1.919523	1.919466	1.919340	1.914567	1.917168
					1.821156	**1.824076**	**1.826590**	**1.814764**	**1.817897**	**1.824866**
		45°			1.836510	1.832149	1.812552	1.831275	1.826952	1.810307
90°	2		1	0.05	**1.765684**	**1.766332**	**1.746882**	**1.758911**	**1.759797**	**1.744892**
		60°			1.774467	1.770109	1.735968	1.769004	1.764741	1.733767
					1.726459	**1.725402**	**1.689868**	**1.719418**	**1.718614**	**1.687687**
		90°			1.624683	1.619430	1.547370	1.618667	1.613641	1.545299
					1.631762	**1.626246**	**1.549813**	**1.624072**	**1.618842**	**1.547159**
			0		1.624683	1.619430	1.547370	1.618667	1.613641	1.545299
					1.631762	**1.626246**	**1.549813**	**1.624072**	**1.618842**	**1.547160**
90°	2	45°	0.5	0.05	1.730596	1.726110	1.681291	1.724971	1.720620	1.679124
					1.698723	**1.696410**	**1.649211**	**1.691492**	**1.689443**	**1.646893**
			1.0		1.836510	1.832149	1.812552	1.831275	1.826952	1.810307
					1.765684	**1.766332**	**1.746882**	**1.758911**	**1.759797**	**1.744892**
				0	1.711297	1.707933	1.702611	1.711297	1.707933	1.702611
					1.638904	**1.640693**	**1.640632**	**1.638904**	**1.640693**	**1.64632**
				0.05	1.836510	1.832149	1.812552	1.831275	1.826952	1.810307
					1.765684	**1.766332**	**1.746882**	**1.758911**	**1.759797**	**1.744892**
90°	2	45°	1	0.10	1.977018	1.971611	1.935794	1.965495	1.960183	1.930711
					1.908539	**1.907940**	**1.866381**	**1.893818**	**1.893718**	**1.861879**
				0.15	2.135823	2.129300	2.074936	2.116834	2.110481	2.066369
					2.070615	**2.068625**	**2.001748**	**2.046612**	**2.045417**	**1.994148**
				0.20	2.316724	2.308987	2.233266	2.288917	2.281448	2.220487
					2.255900	**2.252330**	**2.156294**	**2.221065**	**2.218627**	**2.144921**

V. CONCLUSION

The present study investigates the numerical solution of unsteady aligned MHD flow of magnetic nanofluids over an inclined plate with leading edge accretion. The non-linear governing partial differential equations are transformed using suitable transformations and solved numerically by finite difference scheme. Physically, the effect of magnetic interaction parameter, M, magnetic field inclination angle, α, free convection parameter, Gr_x and nanoparticles volume fraction, ϕ were studied in detail and the results are discussed graphically and in tabular. The main findings of this study can be summarized as follows:

- Velocity increases as α, M and Gr_x increase for $\omega = 0°, 45°$ and $90°$.
- Velocity decreases with the increase in ϕ for $\omega = 0°, 45°$ and $90°$.
- Temperature increases with the increase in ϕ for $\omega = 0°, 45°$ and $90°$.

- Temperature decreases with the increase in α, M and Gr_x for $\omega = 45°$ and $90°$, while unchanged for $\omega = 0$.
- Local skin friction increases with the increase in α, M Gr_x and ϕ for $\omega = 0°, 45°$ and $90°$.
- Reduced Nusselt number increases with the increase in α, M and Gr_x for $\omega = 45°$ and $90°$, while unchanged for $\omega = 0$.
- Reduced Nusselt number increases with the increase in ϕ for $\omega = 0°, 45°$ and $90°$.

CONFLICT OF INTEREST

The authors declare no conflict of interest.

ACKNOWLEDGEMENTS

The authors would like to acknowledge Ministry of Education (MOE) and Research Management Centre-UTM for the financial support through vote numbers 4F713, 4F538 and 06H67 for this research.

TABLE V. VARIATION IN NUSSELT NUMBER FOR MAGNETIC NANOFLUIDS AND NON-MAGNETIC NANOFLUIDS AT DIFFERENT PARAMETERS.

α	M	γ	Gr_x	ϕ	Fe_3O_4-water **Fe_3O_4-kerosene**			Al_2O_3-water **Al_2O_3-kerosene**		
					$\omega = 0°$	$\omega = 45°$	$\omega = 90°$	$\omega = 0°$	$\omega = 45°$	$\omega = 90°$
0°	2	45°	1	0.05	1.478101	1.377195	0.805663	1.496604	1.394385	0.817543
					2.845697	**2.537746**	**1.219770**	**2.839373**	**2.530184**	**1.214817**
45°					1.478101	1.421785	0.922657	1.496604	1.440854	0.937787
					2.845697	**2.606203**	**1.468669**	**2.839373**	**2.600718**	**1.468405**
70°					1.478101	1.442014	0.966007	1.496604	1.461653	0.981889
					2.845697	**2.638701**	**1.556824**	**2.839373**	**2.633717**	**1.557016**
90°					1.478101	1.447055	0.976325	1.496604	1.466820	0.992367
					2.845697	**2.646955**	**1.577788**	**2.839373**	**2.642070**	**1.578050**
90°	0	45°	1	0.05	1.478101	1.377195	0.805663	1.496604	1.394385	0.817543
					2.845697	**2.537746**	**1.219770**	**2.839373**	**2.530184**	**1.214817**
	1				1.478101	1.421785	0.922657	1.496604	1.440854	0.937787
					2.845697	**2.606203**	**1.488669**	**2.839373**	**2.600718**	**1.468405**
	2				1.478101	1.447055	0.976325	1.496604	1.466820	0.992367
					2.845697	**2.646955**	**1.577788**	**2.839373**	**2.642070**	**1.578050**
	4				1.478101	1.478655	1.037842	1.496604	1.499093	1.054726
					2.845697	**2.700235**	**1.703578**	**2.839373**	**2.695815**	**1.704047**
90°	2	0°	1	0.05	1.478101	1.452063	0.990266	1.496604	1.471966	1.006577
					2.845697	**2.651365**	**1.594501**	**2.839373**	**2.646537**	**1.594864**
		45°			1.478101	1.447055	0.976325	1.496604	1.466820	0.992367
					2.845697	**2.646955**	**1.577788**	**2.839373**	**2.642070**	**1.578050**
		60°			1.478101	1.443474	0.966108	1.496604	1.463139	0.981952
					2.845697	**2.643817**	**1.565625**	**2.839373**	**2.638892**	**1.565812**
		90°			1.478101	1.434686	0.940053	1.496604	1.454107	0.955397
					2.845697	**2.636175**	**1.534959**	**2.839373**	**2.631149**	**1.534955**
90°	2	45°	0	0.05	1.478101	1.434686	0.940053	1.496604	1.454107	0.955397
					2.845697	**2.636175**	**1.534959**	**2.839373**	**2.631149**	**1.534955**
			0.5		1.478101	1.440921	0.958689	1.496604	1.460516	0.974391
					2.845697	**2.641589**	**1.556840**	**2.839373**	**2.636634**	**1.556974**
			1.0		1.478101	1.447055	0.976325	1.496604	1.466820	0.992367
					2.845697	**2.646955**	**1.577788**	**2.839373**	**2.642070**	**1.578050**
90°	2	45°	1	0	1.404848	1.374407	0.928540	1.404848	1.374407	0.928540
					2.585611	**2.406163**	**1.441623**	**2.585611**	**2.406163**	**1.441623**
				0.05	1.478101	1.447055	0.976325	1.496604	1.466820	0.992367
					2.845697	**2.646955**	**1.577788**	**2.839373**	**2.642070**	**1.578050**
				0.10	1.552537	1.520241	1.023458	1.590132	1.560461	1.056104
					3.119794	**2.899569**	**1.717905**	**3.106940**	**2.889650**	**1.718604**
				0.15	1.628552	1.594241	1.069992	1.686252	1.656036	1.120119
					3.409808	**3.165522**	**1.862384**	**3.390550**	**3.150759**	**1.863948**
				0.20	1.706560	1.669331	1.115952	1.785846	1.754297	1.184779
					3.717966	**3.446583**	**2.011671**	**3.692810**	**3.427551**	**2.014810**

REFERENCES

[1] S. K. Das, et al., *Nanofluids: Science and Technology*, John Wiley & Sons, 2007.

[2] J. Buongiorno, "Convective transport in nanofluids," *Journal of Heat Transfer*, vol. 128, no.3, pp. 240-250, 2006.

[3] W. Yu, et al., "Review and comparison of nanofluid thermal conductivity and heat transfer enhancements," *Heat Transfer Engineering*, vol. 29, no. 5, pp. 432-460, 2008.

[4] P. A. Davidson, *An Introduction to Magnetohydrodynamics*, vol. 25, Cambridge university press, 2001.

[5] M. Sheikholeslami and D. M. Davood, "Ferrohydrodynamic and magnetohydrodynamic effects on ferrofluid flow and convective heat transfer," *Energy*, vol. 75, pp. 400-410, 2014.
[6] M. Sheikholeslami and G. B. Mofid, "Free convection of ferrofluid in a cavity heated from below in the presence of an external magnetic field," *Powder Technology*, vol. 256, pp. 490-498, 2014.
[7] A. Jafari, et al., "Simulation of heat transfer in a ferrofluid using computational fluid dynamics technique," *International Journal of Heat and Fluid Flow*, vol. 29, no.4, pp. 1197-1202, 2008.
[8] E. M. Sparrow, R. Eichhorn and J. L. Gregg, "Combined forced and free convection in a boundary layer flow," *The Physics of Fluids*, vol. 2, no.3, pp. 319-328, 1959.
[9] A. Mucoglu and T. S. Chen, "Mixed convection on inclined surfaces," *Journal of Heat Transfer*, vol. 101, no. 3, pp. 422-426, 1979.
[10] C. Ping, "Combined free and forced convection flow about inclined surfaces in porous media," *International Journal of Heat and Mass Transfer*, vol. 20, no. 8, pp. 807-814, 1977.
[11] H. M. Ramadan and J. C. Ali, "Hydromagnetic free convection of a particulate suspension from a permeable inclined plate with heat absorption for non-uniform particle-phase density," *Heat and Mass Transfer*, vol. 39, no. 5, pp. 367-374, 2003.
[12] M. S. Alam, M. M. Rahman, and M. A. Sattar, "MHD free convective heat and mass transfer flow past an inclined surface with heat generation," *Thammasat International Journal of Science and Technology*, vol. 11, no.4, pp. 1-8, 2006.
[13] O. Aydın and K. Ahmet, "MHD mixed convective heat transfer flow about an inclined plate," *Heat and Mass Transfer*, vol. 46, no.1, pp.129, 2009.
[14] N. F. M. Noor, S. Abbasbandy, and H. Ishak, "Heat and mass transfer of thermophoretic MHD flow over an inclined radiate isothermal permeable surface in the presence of heat source/sink," *International Journal of Heat and Mass Transfer*, vol. 55, no.7, pp. 2122-2128, 2012.
[15] S. P. A. Devi and P. Suriyakumar, "Effect of magnetic field on Blasius and Sakiadis flow of nanofluids past an inclined plate," *Journal of Taibah University for Science*, 2017.
[16] C. H. Chen, "Heat and mass transfer in MHD flow by natural convection from a permeable, inclined surface with variable wall temperature and concentration," *Acta Mechanica*, vol. 172, no. 3, pp. 219-235, 2004.
[17] M. A. Seddeek, "The effect of variable viscosity on hydromagnetic flow and heat transfer past a continuously moving porous boundary with radiation," *International Communications in Heat and Mass Transfer*, vol. 27, no. 7, pp. 1037-1046, 2000.
[18] P. Ganesan and G. Palani, "Finite difference analysis of unsteady natural convection MHD flow past an inclined plate with variable surface heat and mass flux," *International Journal of Heat and Mass Transfer*, vol. 47, no. 19, pp. 4449-4457, 2004.
[19] L. Todd, "A family of laminar boundary layers along a semi-infinite flat plate," *Fluid Dynamics Research*, vol. 19, no. 4, pp. 235-249, 1997.
[20] T. Fang, "A note on the unsteady boundary layers over a flat plate," *International Journal of Non-Linear Mechanics*, vol. 43, no. 9, pp. 1007-1011, 2008.
[21] R. J. Tiwari and M. K. Das. "Heat transfer augmentation in a two-sided lid-driven differentially heated square cavity utilizing nanofluids," *International Journal of Heat and Mass Transfer*, vol. 50, no. 9, pp. 2002-2018, 2007.
[22] H. C. Brinkman, "The viscosity of concentrated suspensions and solutions," *The Journal of Chemical Physics*, vol. 20, no. 4, pp. 571-571, 1952.
[23] T. Fang, Z. Ji, and Y. Shanshan, "A new family of unsteady boundary layers over a stretching surface," *Applied Mathematics and Computation*, vol. 217, no. 8, pp. 3747-3755, 2010.
[24] R. A. Van Gorder and K. Vajravelu, "Unsteady boundary layers: Convective heat transfer over a vertical flat plate," *The ANZIAM Journal*, vol. 50, no.4, pp. 541-549, 2009.
[25] K. T., Stewartson, "On the impulsive motion of a flat plate in a viscous fluid," *The Quarterly Journal of Mechanics and Applied Mathematics* , vol. 4, no. 2, pp. 182-198, 1951.
[26] H. B. Keller, *A New Difference Scheme for Parabolic Problems, Numerical Solutions of Partial Differential Equations*, Academic Press, New York, 1971.
[27] T. Cebeci and P. Bradshaw, *Physical and Computational Aspects of Convective Heat Transfer*, Springer Science & Business Media, 2012.
[28] M. Sheikholeslami, D. G. Davood, and M. R. Mohammad, "Ferrofluid flow and heat transfer in a semi annulus enclosure in the presence of magnetic source considering thermal radiation," *Journal of the Taiwan Institute of Chemical Engineers*, vol. 47, pp. 6-17, 2015.
[29] H. F. Oztop and A. N. Eiyad, "Numerical study of natural convection in partially heated rectangular enclosures filled with nanofluids," *International Journal of Heat and Fluid Flow*, vol. 29, no. 5, pp. 1326-1336, 2008.
[30] P. Ram and K. Vikas, "Swirling flow of field dependent viscous ferrofluid over a porous rotating disk with heat transfer," *International Journal of Applied Mechanics*, vol. 6, no. 04, pp. 1450033, 2014.
[31] A. Bejan, *Convection Heat Transfer*, John Wiley & Sons, 2013.
[32] L. Colla, et al., "Water-based Fe_2O_3 nanofluid characterization: thermal conductivity and viscosity measurements and correlation," *Advances in Mechanical Engineering*, vol. 4, pp. 674947, 201